Seeding Crystallization in Time

Michal Hajdušek[●],[1,2,*] Parvinder Solanki[●],[3] Rosario Fazio,[4,5] and Sai Vinjanampathy[3,6,†]

[1]*Shonan Fujisawa Campus, Keio University, 5322 Endo, Fujisawa, Kanagawa 252-0882, Japan*
[2]*Quantum Computing Center, Keio University, 3-14-1 Hiyoshi, Kohoku, Yokohama, Kanagawa 223-8522, Japan*
[3]*Department of Physics, Indian Institute of Technology-Bombay, Powai, Mumbai 400076, India*
[4]*The Abdus Salam International Center for Theoretical Physics (ICTP), Strada Costiera 11, 34151 Trieste, Italy*
[5]*Dipartimento di Fisica, Università di Napoli Federico II, Monte S. Angelo, I-80126 Napoli, Italy*
[6]*Centre for Quantum Technologies, National University of Singapore, 3 Science Drive 2, 117543 Singapore, Singapore*

We introduce the concept of seeding of crystallization in time by studying the dynamics of an ensemble of coupled continuous time crystals. We demonstrate that a single subsystem in a broken-symmetry phase acting as a nucleation center may induce time-translation symmetry breaking across the entire ensemble. Seeding is observed for both coherent and dissipative coupling, as well as for a broad range of parameter regimes. In the spirit of mutual synchronization, we investigate the parameter regime where all subsystems are in the broken-symmetry phase. We observe that more broadly detuned time crystals require weaker coupling strength to be synchronized. This is in contrast to basic knowledge from classical as well as quantum synchronization theory. We show that this surprising observation is a direct consequence of the seeding effect.

Introduction.—Time crystals are nonequilibrium phases of matter with broken time-translation symmetry [1,2]. Initial theoretical investigations [3–10] and experimental demonstrations so far [11–17] focused on breaking of the *discrete* time-translation symmetry in closed systems, followed soon after by dissipative systems as well [18–22]. Introducing dissipation led to the "continuous time crystals" (CTCs) [23–31]. Here, the continuous time-translation symmetry is broken in the thermodynamic limit when a self-organized steady state emerges with period of oscillation depending only on the system parameters. Emergence of global oscillations in coupled classical systems has been extensively investigated, particularly in chemistry [32,33] and biology [34,35] in the context of quorum sensing [36]. Inspired by the growth of broken-symmetry phases in classical phase transitions by seeding a crystal in a solution [37], we investigate the following question. Can the broken time-translation symmetry of a seeding crystal induce time crystallization of the entire system in a similar fashion? We answer this question in the affirmative and demonstrate that seeding of crystallization in time is, indeed, not only possible but, under certain conditions, inevitable.

We investigate a network of n interacting CTCs where all but one subsystem are in the unbroken-symmetry phase. We derive the required conditions under which the time-translation symmetry breaking permeates across the entire system. We consider the thermodynamic limit and also demonstrate that this effect occurs for finite timescales in the finite-size scenario. We analyze the eigenspectrum of

the generator of dynamics to understand the mechanism of crystallization of time. Furthermore, in the spirit of mutual synchronization [38], we consider the dynamics of the subsystems in the broken-symmetry phase but oscillating at different natural frequencies. We obtain the phase diagram of when synchronization of the two subsystems occurs and find that farther detuned oscillators can be more easily synchronized. This is in stark contrast to current understanding of synchronization in both classical as well as quantum systems. We show that this surprising behavior is a direct consequence of the seeding effect. In particular, we show that weakly coupled subsystems oscillate with distinct observed frequencies, but upon reaching a critical coupling one of the subsystems begins to seed oscillations from the other, leading to synchronized dynamics.

Seeding crystallization.—Before exploring a concrete example, we establish the general signatures of seeding of crystallization in time both in the thermodynamic limit as well as in the finite-size case. Spontaneous symmetry breaking in a CTC is witnessed by the emergence of transient oscillations of an order parameter $\langle \hat{O} \rangle$ for finite size. These oscillations become persistent in the thermodynamic limit [23] when the system size diverges. Development of such persistent oscillations in generic driven dissipative systems is not guaranteed and depends on the interplay of coherent and dissipative dynamics, characterized by parameters Ω and κ, respectively. Dynamics of such a system is governed by a Liouvillian superoperator,
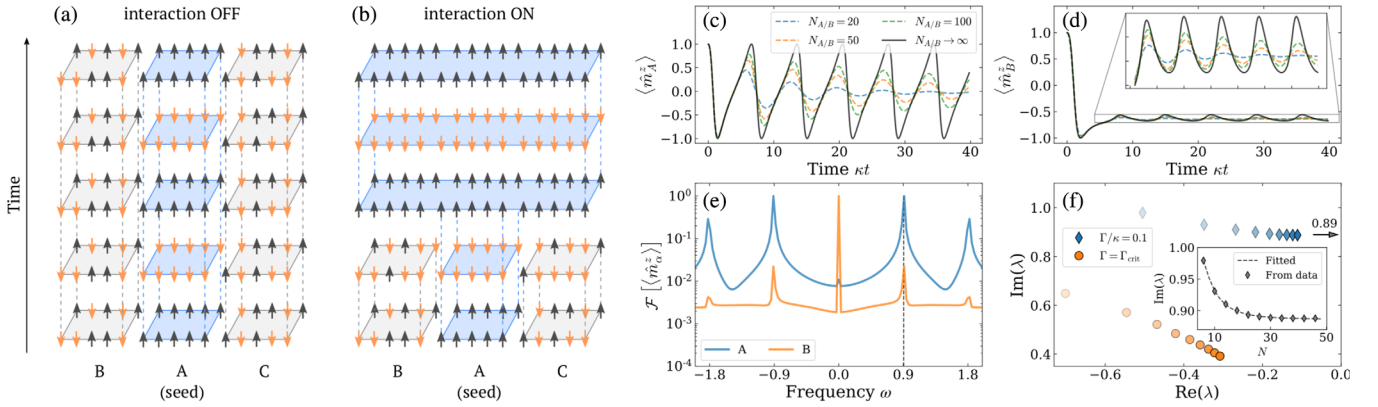
FIG. 1. (a) In the absence of interactions, crystallization (blue regions) does not permeate through the whole system. Subsystems B and C remain time-translationally symmetric. (b) When interaction is turned on, ensemble A seeds crystallization to ensembles B and C after some initial transient. (c),(d) Time evolution of $\langle \hat{m}_\alpha^z \rangle$ for two subsystems A (seed) and B for finite size and the thermodynamic limit. Parameters are $\Omega_A/\kappa = 1.5$, $\Omega_B/\kappa = 0.9$, and $\Gamma/\kappa = 0.1$. (e) Normalized Fourier transform of $\langle \hat{m}_\alpha^z \rangle$. The coinciding peaks show that B is phase locked to A. (f) Scaling of the dominant eigenvalue of the Liouville eigenspectrum for finite-sized subsystems when $N = \{6, 10, 14, 18, 22, 26, 30, 34, 38\}$. Increasing color saturation of the points represents increasing system size. Blue diamonds represent coupling of $\Gamma/\kappa = 0.1 < \Gamma_{\text{crit}}/\kappa$ and seeding occurs. The inset shows functional scaling of $\text{Im}(\lambda)$ and sits convergence to 0.89. The orange circles represent the case of critical coupling Γ_{crit} when both subsystems are in the unbroken-symmetry phase. The real part of the dominant eigenvalue does not vanish anymore.

$$\dot{\rho} = L_{\text{CTC}}[\Omega, \kappa](\rho). \qquad (1)$$

Specific examples of such models are considered below. In a Dicke model of the CTC [23] crystallization occurs in the weakly dissipative regime, $\Omega/\kappa > 1$, while the system remains time-translationally invariant in the strongly dissipative regime, $\Omega/\kappa \leq 1$.

Consider a network of n coupled CTCs evolving according to

$$\dot{\rho} = \sum_\alpha L_{\text{CTC}}[\Omega_\alpha, \kappa_\alpha](\rho) + L_V[\Gamma](\rho), \qquad (2)$$

where α indexes the subsystem and $L_V[\Gamma](\rho)$ describes their interaction at strength Γ. All subsystems are in the strongly dissipative regime, except for the seed, which is set to be in the broken-symmetry phase, $\Omega_{\text{seed}}/\kappa_{\text{seed}} > 1$. In the thermodynamic limit, seeding is witnessed by oscillating order parameters $\langle \hat{O}_\alpha \rangle$ signifying a broken-symmetry phase for any subsystem α. Figures 1(a) and 1(b) illustrate this idea with an example of three subsystems, where A is the seed.

For finite subsystems, the time-translation symmetry is broken for finite timescales before the order parameter oscillations vanish (even for the seed). A suitable tool for analyzing this scenario is the spectrum of the Liouville superoperator, denoted by complex eigenvalues λ_j, generating the dynamics of the system [20,23,39–42]. The transient oscillations of the order parameter are a consequence of finite imaginary parts of the eigenvalues, $\text{Im}(\lambda_j) \neq 0$, while their damping is the result of negative real parts, $\text{Re}(\lambda_j) < 0$. Witnessing seeding in this case amounts to requiring the imaginary part of the Liouville

eigenspectrum to remain gapped while its real part becomes gapless as the subsystem's size increases.

Model.—Consider n subsystems indexed by α, each composed of N_α spin-1/2 atoms with total spin $S_\alpha = N_\alpha/2$. The spins undergo collective dissipation at rates κ_α/S_α and are pumped coherently with strength Ω_α. We now make a particular choice for the interaction $L_V[\Gamma]$ in Eq. (2) and discuss other interactions later. We assume the subsystems interact dissipatively at rate Γ/S, where $S = \sum_\alpha S_\alpha$. Evolution of the total system is described by the following master equation (see the Supplemental Material [44]),

$$\dot{\rho} = \sum_\alpha \left\{ -i[\Omega_\alpha \hat{S}_\alpha^x, \rho] + \frac{\kappa_\alpha}{S_\alpha} \mathcal{D}[\hat{S}_\alpha^-]\rho \right\} + \frac{\Gamma}{S} \mathcal{D}[\hat{S}^-]\rho, \quad (3)$$

where $\hat{S}_\alpha^k = \frac{1}{2}\sum_j \hat{\sigma}_{\alpha,j}^k$ are the collective spin operators for $k = x, y, z$ and subsystem α, and $\hat{S}_\alpha^- = \hat{S}_\alpha^x - i\hat{S}_\alpha^y$ and $\hat{S}^- = \sum_\alpha \hat{S}_\alpha^-$ are the collective annihilation operators. The dissipators are given in Lindblad form as $\mathcal{D}[\hat{O}]\rho = \hat{O}\rho\hat{O}^\dagger - \frac{1}{2}\{\hat{O}^\dagger\hat{O}, \rho\}$. For simplicity, we consider the subsystems with $\kappa_\alpha = \kappa$ and $S_\alpha = S_\beta$.

We begin with an analysis of Eq. (3) in the thermodynamic limit. Note that the rescaled spin operators $\hat{m}_\alpha^k \equiv \hat{S}_\alpha^k/S_\alpha$, obey the commutation relation $[\hat{m}_\alpha^k, \hat{m}_\alpha^l] = i\varepsilon^{klm}\hat{m}_\alpha^m/S_\alpha$, where ε^{klm} is the Levi-Civita symbol. In the thermodynamic limit when $S_\alpha \to \infty$, these operators commute and their two-point correlation functions factorize [23], leading to a system of classical nonlinear dynamical equations for the expectation values $\langle \hat{m}_\alpha^k \rangle$ (see the Supplemental Material [44]).

Consider the case of $n = 2$ subsystems labeled by A and B, respectively. Subsystem A is the seed with $\Omega_A/\kappa > 1$, while subsystem B is set in the strongly dissipative regime with $\Omega_B/\kappa < 1$. In the absence of coupling, only A breaks the time-translation symmetry. Introducing weak coupling induces symmetry breaking in subsystem B as depicted in Figs. 1(c) and 1(d) where we plot $\langle \hat{m}_A^z \rangle$ and $\langle \hat{m}_B^z \rangle$, respectively. In the finite-size case, oscillations of A and B are transient but become persistent limit-cycle oscillations when $N_{A/B} \to \infty$ as expected from [23]. Furthermore, we observe the induced oscillations in ensemble B are phase locked to the oscillations in A by examining the Fourier transform $\mathcal{F}[\langle \hat{m}_\alpha^z \rangle]$ in Fig. 1(e).

It is important to note the role of dissipation in breaking the time-translation symmetry. In the case of a single subsystem considered in [23], the limit-cycle oscillations are a result of the interplay between coherent driving producing oscillations and collective dissipation, causing the damping of these oscillations. Stable limit cycles emerge only once the coherent drive overcomes the dissipation and $\Omega_\alpha/\kappa > 1$. Therefore, it is surprising that limit-cycle oscillations in Fig. 1(d) are seeded via dissipative coupling. Furthermore, seeding occurs for arbitrarily small Γ/κ, albeit producing only arbitrarily small oscillations.

Increasing the coupling strength also increases the amplitude of seeded oscillations provided the coupling is below a certain critical strength, $\Gamma < \Gamma_{\text{crit}}$. Beyond this critical coupling, both subsystems enter the unbroken-symmetry phase. This critical coupling Γ_{crit} can be obtained via linear stability analysis (see Supplemental Material [44]),

$$\Gamma_{\text{crit}} = \frac{2\kappa(\Omega_A - \kappa)}{2\kappa - (\Omega_A - \Omega_B)}, \qquad (4)$$

where $\Omega_A > \Omega_B$. We note that increasing the coherent driving strength of the seed Ω_A results in larger critical coupling for a fixed Ω_B. This, in turn, allows the subsystems to be coupled more strongly before entering the unbroken-symmetry phase.

In Fig. 1(f), we show scaling of the dominant eigenvalue of the Liouvillian spectrum for increasing subsystem size. For subcritical coupling, $\text{Re}(\lambda)$ converges to zero, while $\text{Im}(\lambda)$ saturates to a finite value predicted by the mean-field analysis indicated by a black arrow. For critical coupling, λ converges to a large negative component, indicating absence of a broken-symmetry phase. The asymptotic eigenvalues were determined by fitting numerical eigenvalues to a large-N_α expansion with free coefficients, as shown in Sec. C of the Supplemental Material [44]. We also verified that in the case of oscillating coherences the next dominant eigenvalue indeed saturates to a nonzero real value with a large gap (see [44]). To further corroborate our results, we plot time-dependent oscillations for up to
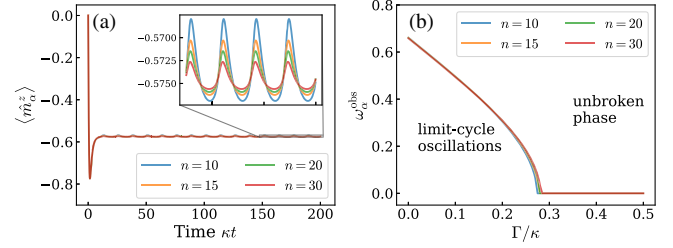

FIG. 2. (a) Seeding of crystallization in time for a single seed with $\Omega_{\text{seed}}/\kappa = 1.2$ and $n - 1$ subsystems set in the unbroken-symmetry phase, $\Omega_\alpha/\kappa = 0.9$ for all α, with coupling strength $\Gamma/\kappa = 0.1$. Seeding can be observed for all subsystems α with identical limit-cycle oscillations of $\langle \hat{m}_\alpha^z \rangle$. (b) Observed frequency $\omega_\alpha^{\text{obs}}$ vanishes beyond a critical coupling, signifying all subsystems entering the unbroken phase.

$N_{A/B} = 100$, which oscillate with frequency predicted by the mean field, as shown in Figs. 1(c) and 1(d).

We now expand our discussion of seeding to n ensembles. We consider a single seed and $n - 1$ subsystems in the unbroken-symmetry phase. Figure 2(a) shows that seeding is observed even for large numbers of subsystems. The amplitude of limit-cycle oscillations decreases with increasing n as seen in the inset of Fig. 2(a). Increasing the coupling strength Γ/κ has the effect of boosting this amplitude; however, beyond a critical coupling the dissipation becomes unsustainable and limit-cycle oscillations vanish. This can be seen in Fig. 2(b) where we plot the *observed* frequency defined as $\omega_\alpha^{\text{obs}} = 2\pi/T_\alpha$, where T_α is the period of oscillation for subsystem α. The observed frequencies of the $n - 1$ subsystems follow the frequency of the seed, which decreases with increasing coupling strength Γ and vanishes upon reaching the critical coupling strength Γ_{crit}. Note that this critical coupling depends on the number of subsystems n.

Until this point, we have discussed dissipative coupling of Eq. (3) only. Seeding of crystallization is observed for coherent exchange interaction of the form $\hat{S}_\alpha^+ \hat{S}_\beta^- + \hat{S}_\alpha^- \hat{S}_\beta^+$. The qualitative features of seeding for this type of coupling are the same as for dissipative coupling described above (see the Supplemental Material [44]).

Synchronization.—We now consider the dynamics of Eq. (3) with $n = 2$, where both subsystems are in the broken-symmetry phase displaying limit-cycle oscillations with different observed frequencies, $\omega_A^{\text{obs}} \neq \omega_B^{\text{obs}}$, achieved by setting $\Omega_A \neq \Omega_B$. In the rest of this section, $\Omega_A - \Omega_B$ serves as a convenient measure of detuning between the subsystems.

We are interested in the dynamics of the coupled system, in particular, how the observed frequency $\omega_\alpha^{\text{obs}}$ changes with varying coupling strength and detuning in anticipation of observing synchronization. This requires a suitable quantifier of how synchronized the two subsystems are. Recent years have seen a substantial effort to develop tools to quantify synchronization in quantum systems [43,45]. An intuitive measure of synchronization for such
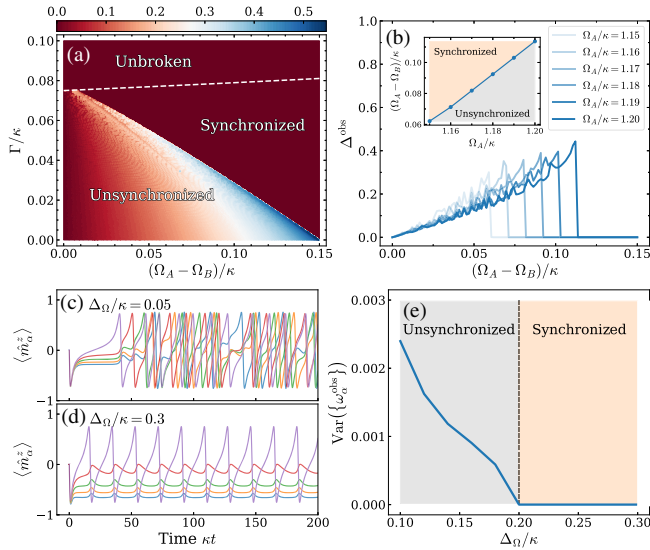
FIG. 3. (a) Δ^{obs} indicating the synchronization region for $n = 2$ and $\Omega_A/\kappa = 1.15$. The white dashed curve is the critical coupling from Eq. (4). (b) Increasing Ω_A/κ also increases the minimum detuning required in order to observe synchronization. The coupling strength is kept at $\Gamma/\kappa = 0.05$. (c),(d) Time evolution of $\langle \hat{m}_\alpha^z \rangle$ for detuning range $\Delta_\Omega/\kappa = 0.05$ and 0.3, respectively. (e) Variance of the observed frequencies $\text{Var}(\{\omega_\alpha^{\text{obs}}\})$ vanishes when the detuning interval Δ_Ω/κ is high enough, indicating synchronized dynamics. Parameters for (c)–(e) are $n = 5$, $\max\{\Omega_\alpha/\kappa\} = 1.5$, and $\Gamma/\kappa = 0.5$.

mean-field analysis is the magnitude of the difference between observed frequencies of the two subsystems,

$$\Delta^{\text{obs}} = |\omega_A^{\text{obs}} - \omega_B^{\text{obs}}|. \tag{5}$$

It is straightforward to see that if the limit-cycle oscillations of both subsystems are synchronized, then Δ^{obs} vanishes and is positive otherwise.

Figure 3(a) shows Δ^{obs} as a function of the detuning $(\Omega_A - \Omega_B)/\kappa$ and the coupling strength Γ/κ. The driving strength of subsystem A is fixed to $\Omega_A/\kappa = 1.15$ and we vary Ω_B. For reference, we also plot the critical driving strength $\Gamma_{\text{crit}}/\kappa$ of Eq. (4) beyond which both subsystems enter the strongly dissipative regime.

In Fig. 3(a), we display the synchronization measure as a function of detuning and coupling strength. We observe that larger detuning, given by large $(\Omega_A - \Omega_B)/\kappa$, requires weak coupling strength Γ/κ to produce synchronization of the two subsystems. On the other hand, stronger coupling must be applied when the two subsystems are weakly detuned in order to synchronize them. We believe this is the first time such behavior has been observed. This is in contrast with countless examples of classical and quantum synchronizing dynamics studied in literature that share a common property, namely, that small detuning requires weak coupling in order to produce synchronization, while large detuning requires stronger coupling [38,46–49].

We now show that this unusual observation can be explained using seeding of crystallization. Consider a particular detuning in Fig. 3(a) where $\Omega_A > \Omega_B$. For weak coupling Γ/κ the oscillations of both subsystems are unsynchronized. Increasing the coupling strength has two effects. It affects the observed frequency of oscillations of the subsystems on one hand, but also acts as a new source of dissipation countering the effect of coherent drives Ω_A and Ω_B. Therefore, increasing the coupling strength eventually forces subsystem B into a regime where the coherent drive Ω_B is not strong enough to sustain its oscillations. At this point, subsystem A starts seeding oscillations to subsystem B, forcing it to lock to its frequency of oscillations as previously seen in Fig. 1(e).

Seeding of crystallization as the mechanism behind synchronization of CTCs has another consequence. The shape of the phase diagram in Fig. 3(a) depends not only on the detuning and the coupling strength, but also on the coherent driving strengths Ω_A and Ω_B. To see this, we fix the coupling strength Γ/κ and increase the coherent drive strength Ω_A/κ. We expect that stronger coherent drive Ω_A/κ has the effect of shifting the boundary between unsynchronized and synchronized dynamics toward larger values of detuning $(\Omega_A - \Omega_B)/\kappa$. In Fig. 3(b), we show Δ^{obs} as a function of the detuning between the CTCs for increasing values of Ω_A/κ. We observe that increasing Ω_A/κ for a fixed coupling strength Γ/κ produces larger minimum detuning $(\Omega_A - \Omega_B)/\kappa$ required for synchronization as depicted in the inset of Fig. 3(b). This confirms our expectation.

We now turn to the case of multiple subsystems, each with its own coherent drive strength Ω_α picked from a detuning range Δ_Ω. Without loss of generality we assume that the set $\{\Omega_\alpha\}$ is distributed uniformly within Δ_Ω in steps of $\Delta_\Omega/(n - 1)$. Figures 3(c) and 3(d) display the time evolution of $\langle \hat{m}_\alpha^z \rangle$ for $n = 5$ subsystems. When the detuning interval Δ_Ω is small, meaning the subsystems are only weakly detuned, no synchronization is observed, as seen in Fig. 3(c). Increasing Δ_Ω beyond a critical value produces synchronization in the whole system, as seen in Fig. 3(d). Generalization of the synchronization measure in Eq. (5) is given by the variance of the observed frequencies $\text{Var}(\{\omega_\alpha^{\text{obs}}\})$, which vanishes when the subsystems become synchronized and is finite otherwise. Figure 3(e) shows $\text{Var}(\{\omega_\alpha^{\text{obs}}\})$ for fixed coupling strength Γ/κ and increasing detuning intervals Δ_Ω, indicating clearly the transition from unsynchronized dynamics when the subsystems are weakly detuned to synchronized dynamics for large detunings.

Such counterintuitive behavior is not observed when the subsystems are coupled coherently. In this case, slightly detuned subsystems require weak coupling to synchronize their dynamics, while large detuning demands strong coupling, conforming to the usual behavior in synchronization theory.

Conclusions.—Crystal structure and its formation is one of the fundamental aspects of understanding the solid state. The ability for nucleation centers to seed crystallization in a solute and its role in spontaneous spatial symmetry breaking has been appreciated for a long time. Results presented in this Letter contribute toward understanding the foundations of spontaneous continuous time-translation symmetry breaking in coupled systems, an area which has gone underexplored so far. Seeding of crystallization in time is not only possible but in many cases inevitable, as it occurs for both coherent as well as dissipative coupling and a broad range of parameters. The role of dissipation in spontaneous time-translation breaking is to destroy persistent limit-cycle oscillations. It is therefore surprising that dissipative coupling leads to proliferation of broken-symmetry phases through the global system. Given appropriate coupling, we expect that other physical systems, whether displaying continuous or discrete time-translational symmetry breaking, can be used to observe such behavior.

We note that the emergence of oscillations in networks of otherwise quiescent classical oscillators has been investigated in [50]. Unlike the seeding effect discussed in this Letter, the oscillations either spread only to a fraction of the subsystems or are observed only during the transient dynamics. Results presented in this Letter are among the first steps toward understanding similar phenomena in quantum systems.

In the context of mutual synchronization, seeding leads to the extraordinary observation that dissipatively coupled CTCs do not follow the principle tenet of synchronization theory: that increasing detuning requires stronger coupling in order for the subsystems to synchronize. In fact, the precise opposite is true in our case. Conventional and nature-inspired synchronization schemes have numerous practical applications in complex networks [51]. Researchers and engineers go to great lengths designing dynamical systems that are nearly identical in order to facilitate their synchronization in these protocols. Our results show that this is not necessarily needed, opening the path to new design philosophies in network synchronization.

---

[*]michal@sfc.wide.ad.jp
[†]sai@phy.iitb.ac.in

[1] K. Sacha and J. Zakrzewski, Rep. Prog. Phys. **81**, 016401 (2018).

[2] D. V. Else, C. Monroe, C. Nayak, and N. Y. Yao, Annu. Rev. Condens. Matter Phys. **11**, 467 (2020).

[3] K. Sacha, Phys. Rev. A **91**, 033617 (2015).

[4] D. V. Else, B. Bauer, and C. Nayak, Phys. Rev. Lett. **117**, 090402 (2016).

[5] V. Khemani, A. Lazarides, R. Moessner, and S. L. Sondhi, Phys. Rev. Lett. **116**, 250401 (2016).

[6] A. Russomanno, F. Iemini, M. Dalmonte, and R. Fazio, Phys. Rev. B **95**, 214307 (2017).

[7] F. M. Surace, A. Russomanno, M. Dalmonte, A. Silva, R. Fazio, and F. Iemini, Phys. Rev. B **99**, 104303 (2019).

[8] T. L. Heugel, M. Oscity, A. Eichler, O. Zilberberg, and R. Chitra, Phys. Rev. Lett. **123**, 124301 (2019).

[9] R. Khasseh, R. Fazio, S. Ruffo, and A. Russomanno, Phys. Rev. Lett. **123**, 184301 (2019).

[10] A. Sakurai, V. M. Bastidas, W. J. Munro, and K. Nemoto, Phys. Rev. Lett. **126**, 120606 (2021).

[11] S. Pal, N. Nishad, T. S. Mahesh, and G. J. Sreejith, Phys. Rev. Lett. **120**, 180602 (2018).

[12] J. Rovny, R. L. Blum, and S. E. Barrett, Phys. Rev. Lett. **120**, 180603 (2018).

[13] J. Smits, L. Liao, H. T. C. Stoof, and P. van der Straten, Phys. Rev. Lett. **121**, 185301 (2018).

[14] J. Zhang, P. Hess, A. Kyprianidis, P. Becker, A. Lee, J. Smith, G. Pagano, I.-D. Potirniche, A. C. Potter, A. Vishwanath et al., Nature (London) **543**, 217 (2017).

[15] S. Choi, J. Choi, R. Landig, G. Kucsko, H. Zhou, J. Isoya, F. Jelezko, S. Onoda, H. Sumiya, V. Khemani et al., Nature (London) **543**, 221 (2017).

[16] A. Kyprianidis, F. Machado, W. Morong, P. Becker, K. S. Collins, D. V. Else, L. Feng, P. W. Hess, C. Nayak, G. Pagano, N. Y. Yao, and C. Monroe, Science **372**, 1192 (2021).

[17] H. Taheri, A. B. Matsko, L. Maleki, and K. Sacha, arXiv:2012.07927.

[18] Z. Gong, R. Hamazaki, and M. Ueda, Phys. Rev. Lett. **120**, 040404 (2018).

[19] A. Lazarides, S. Roy, F. Piazza, and R. Moessner, Phys. Rev. Research **2**, 022002(R) (2020).

[20] A. Riera-Campeny, M. Moreno-Cardoner, and A. Sanpera, Quantum **4**, 270 (2020).

[21] H. Keßler, P. Kongkhambut, C. Georges, L. Mathey, J. G. Cosme, and A. Hemmerich, Phys. Rev. Lett. **127**, 043602 (2021).

[22] A. Sakurai, V. M. Bastidas, M. P. Estarellas, W. J. Munro, and K. Nemoto, Phys. Rev. B **104**, 054304 (2021).

[23] F. Iemini, A. Russomanno, J. Keeling, M. Schirò, M. Dalmonte, and R. Fazio, Phys. Rev. Lett. **121**, 035301 (2018).

[24] K. Tucker, B. Zhu, R. J. Lewis-Swan, J. Marino, F. Jimenez, J. G. Restrepo, and A. M. Rey, New J. Phys. **20**, 123003 (2018).

[25] B. Buča, J. Tindall, and D. Jaksch, Nat. Commun. **10**, 1730 (2019).

[26] B. Zhu, J. Marino, N. Y. Yao, M. D. Lukin, and E. A. Demler, New J. Phys. **21**, 073028 (2019).

[27] C. Lledó, T. K. Mavrogordatos, and M. H. Szymańska, Phys. Rev. B **100**, 054303 (2019).

[28] K. Seibold, R. Rota, and V. Savona, Phys. Rev. A **101**, 033839 (2020).

[29] L. F. d. Prazeres, L. d. S. Souza, and F. Iemini, Phys. Rev. B **103**, 184308 (2021).

[30] G. Piccitto, M. Wauters, F. Nori, and N. Shammah, Phys. Rev. B **104**, 014307 (2021).

[31] F. Carollo and I. Lesanovsky, arXiv:2110.00030.

[32] M. R. Tinsley, A. F. Taylor, Z. Huang, and K. Showalter, Phys. Rev. Lett. **102**, 158301 (2009).

[33] A. F. Taylor, M. R. Tinsley, F. Wang, Z. Huang, and K. Showalter, Science **323**, 614 (2009).

[34] J. Aldridge and E. K. Pye, Nature (London) **259**, 670 (1976).

[35] S. Danø, P. G. Sørensen, and F. Hynne, Nature (London) **402**, 320 (1999).

[36] H. Singh and P. Parmananda, J. Phys. Chem. A **116**, 10269 (2012).

[37] J. Mullin, *Crystallization* (Elsevier Science, Oxford, 2001), https://www.elsevier.com/books/crystallization/mullin/978-0-7506-4833-2.

[38] A. Pikovsky, J. Kurths, M. Rosenblum, and J. Kurths, *Synchronization: A Universal Concept in Nonlinear Sciences* (Cambridge University Press, New York, 2003), Vol. 12, https://www.cambridge.org/jp/academic/subjects/physics/nonlinear-science-and-fluid-dynamics/synchronization-universal-concept-nonlinear-sciences?format=PB.

[39] V. V. Albert and L. Jiang, Phys. Rev. A **89**, 022118 (2014).

[40] J. Tindall, C. S. Muñoz, B. Buča, and D. Jaksch, New J. Phys. **22**, 013026 (2020).

[41] P. Solanki, N. Jaseem, M. Hajdušek, and S. Vinjanampathy, arXiv:2104.04383.

[42] B. Buča, C. Booker, and D. Jaksch, arXiv preprint arXiv:2103.01808 (2021).

[43] N. Jaseem, M. Hajdušek, P. Solanki, L.-C. Kwek, R. Fazio, and S. Vinjanampathy, Phys. Rev. Research **2**, 043287 (2020).

[44] See Supplemental Material at http://link.aps.org/supplemental/10.1103/PhysRevLett.128.080603 for the master equation derivation, linear stability of the fixed points, large-N expansion analysis, and seeding in the case of coherent coupling.

[45] F. Galve, G. Luca Giorgi, and R. Zambrini, Quantum correlations and synchronization measures, in *Lectures on General Quantum Correlations and their Applications*, edited by F. F. Fanchini, D. d. O. Soares Pinto, and G. Adesso (Springer International Publishing, Cham, 2017), pp. 393–420, 10.1007/978-3-319-53412-1_18.

[46] S. Sonar, M. Hajdušek, M. Mukherjee, R. Fazio, V. Vedral, S. Vinjanampathy, and L.-C. Kwek, Phys. Rev. Lett. **120**, 163601 (2018).

[47] Y. Kato, N. Yamamoto, and H. Nakao, Phys. Rev. Research **1**, 033012 (2019).

[48] A. Cabot, G. L. Giorgi, and R. Zambrini, New J. Phys. **23**, 103017 (2021).

[49] N. Jaseem and M. Hajdušek, V. Vedral, R. Fazio, L.-C. Kwek, and S. Vinjanampathy, Phys. Rev. E **101**, 020201(R) (2020).

[50] A. Biswas, P. Kumar, D. Das, and P. Parmananda, Phys. Rev. E **99**, 032223 (2019).

[51] H.-H. Choi and J.-R. Lee, Mobile Inf. Syst. **2017**, 8932631 (2017).

[52] J. Johansson, P. Nation, and F. Nori, Comput. Phys. Commun. **183**, 1760 (2012).

[53] J. Johansson, P. Nation, and F. Nori, Comput. Phys. Commun. **184**, 1234 (2013).

[54] N. Shammah, S. Ahmed, N. Lambert, S. De Liberato, and F. Nori, Phys. Rev. A **98**, 063815 (2018).